



Cite this: DOI: 10.1039/c7nj02034a

Halogen-bonding contacts determining the crystal structure and fluorescence properties of organic salts†

Jing-Wen Wang, Chen Chen, Yao-Ja Li, Yang-Hui Luo * and Bai-Wang Sun *

By using the ligands 4-(4-bromobenzylideneamino)-4H-1,2,4-triazole (**L**₁) and 4-(4-iodobenzylideneamino)-4H-1,2,4-triazole (**L**₂), four different organic salts **HL**₁⁺·Cl[−] (**1**), **L**₁·**HL**₁⁺·ClO₄[−] (**2**), **HL**₂⁺·Cl[−] (**3**), and **L**₂·**HL**₂⁺·ClO₄[−] (**4**) have been synthesized and structurally characterized through single-crystal X-ray diffraction (**L**₁, **L**₂, **2** and **3**) and PXRD (**1** and **4**) measurements. The results revealed that ligands **L**₁ and **L**₂ themselves exhibit a polymeric 1-D chain in a zigzag structure connected by C–Br···N and C–I···N halogen-bonding contacts, respectively. **L**₁ in salt **2** was connected into a 3-D structure through N–H···O hydrogen-bonding contacts, while the interleaved 3-D network of **L**₂ in salt **3** was mainly connected by C–I···Cl halogen-bonding contacts. As a result, the fluorescence properties of ligands **L**₁ and **L**₂ were reserved in halogen-bonding connected salts **1** and **3**, while there was a reduction in hydrogen-bonding connected salts **2** and **4**. Thus, the relationship between emission properties and halogen-bonding contacts can be proposed.

Received 7th June 2017,
Accepted 20th July 2017

DOI: 10.1039/c7nj02034a

rsc.li/njc

1. Introduction

As is well known, supramolecular engineering strategies rely on noncovalent intermolecular interactions such as van der Waals interactions, hydrogen bonds, and halogen bonds.^{1–3} Although compared to the assembly of supramolecular networks with conventional noncovalent interactions (hydrogen bonding and π ··· π interactions), designed supramolecular crystal engineering with halogen bonding (XB) has been less studied, a lot of emphasis has been put on halogen bonding and supramolecular structures self-assembled using such interaction, particularly in the last 15 years. Interestingly, lots of experimental observations and phenomena, where we are now acknowledging the role played by XB were reported. Additionally, XB was at the core of some important achievements in chemistry, being relevant to the work of R. Mulliken^{4,5} on the chemical bond and central to the conformational studies of O. Hassel.⁶

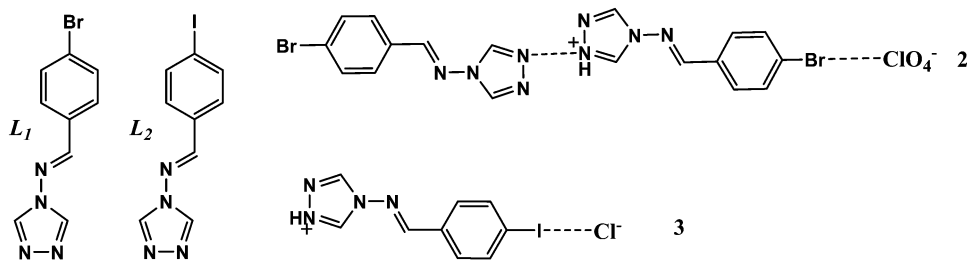
Halogen bonding (discovered in 1863)⁷ with strong n – σ^* interactions and the analogies between XB and HB were valuable in the recent past to understand the features of XB, and the differences between the two interactions may help in the future to identify the specific properties of XB representing added value. For instance, directionality, tunability, hydrophobicity,

and variable size of the donor atom are four unique features of XB, which offer new opportunities if compared to the well-established use of HB.^{8,9} In addition, XB is capable of driving the self-assembly of supramolecular networks¹⁰ and has recently been introduced into solid-state reactivity as well as cocrystallization (superior to other supramolecular interactions),^{11–13} which incredibly opens a new door for chemists to discover the fantastic phenomena in multi-component molecular solids. Thereafter, systematic studies revealed that halogen related interactions, such as X···N (O, S), X··· π and X···X interactions, are ubiquitous, noncovalent interactions in supramolecular engineering. At present, halogen bonds are more widely studied; the formation of XB can develop great potential for high-value, functional materials, most notably in the fields of biological systems,¹⁴ magnetic and conducting materials,¹⁵ non-linear optics (NLO),¹⁶ catalysis¹⁷ and molecular recognition and assembly.¹⁸ However, research on halogen-bonded systems has been primarily focused on crystal engineering^{19,20} rather than on photoluminescence in the past few decades.²¹ This hinders further rational design and preparation of photoluminescent functional halogen-bonded organic salts. Therefore, the photoluminescence characteristics of halogen-bonded solids and their molecule-packing–property relationship currently remain unknown.

Hence, two novel triazolyl Schiff base ligands **L**₁ and **L**₂ (Scheme 1) are selected for their unique p-conjugated system and strong halogen-bonding. Four different molecular salts **HL**₁⁺·Cl[−] (**1**), **L**₁·**HL**₁⁺·ClO₄[−] (**2**), **HL**₂⁺·Cl[−] (**3**), **L**₂·**HL**₂⁺·ClO₄[−] (**4**) have been synthesized and structurally characterized by single-crystal X-ray diffraction (**L**₁, **L**₂, **2** and **3**) and PXRD

School of Chemistry and Chemical Engineering, Southeast University, Nanjing 211189, P. R. China. E-mail: peluoyh@sina.com, chmsunbw@seu.edu.cn; Fax: +86-25-52090614; Tel: +86-25-52090614

† Electronic supplementary information (ESI) available: CCDC 1519856–1519859. For ESI and crystallographic data in CIF or other electronic format see DOI: 10.1039/c7nj02034a



Scheme 1 The molecular structure of ligands L_1 and L_2 and salts **2** and **3**.

(**1** and **4**). By halogen bonding interaction with different anions in the lattice, the stacking modes change greatly, which affords different fluorescence properties in the solid state. These ligands and salts are also characterized through thermogravimetric analyses (TGA), Raman spectroscopy and molecular Hirshfeld surfaces. Meanwhile, their fluorescence properties in solution and in the crystalline state with halogen-bonding contacts were investigated. This research may also help in anticipating future directions.

2. Experimental section

2.1. Materials and physical measurements

All reagents were obtained commercially, and used without further purification. Elemental analyses for carbon, hydrogen and nitrogen were performed using a Vario-EL III elemental analyzer. The infrared spectra (IR) were recorded on a SHIMADZU IR Prestige-21 FTIR-8400S spectrometer as KBr pellets in the range of 4000–400 cm^{-1} . Thermogravimetric analysis (TGA) was performed using a NETZSCH TG 2009 F3 system at a heating rate of 20 K min^{-1} under an atmosphere of dry nitrogen flowing at 20 $\text{cm}^3 \text{min}^{-1}$ over the range from 50 to 500 $^\circ\text{C}$. The UV-vis absorption spectra were recorded on a Shimadzu UV-3600 spectrometer in the range of 200–800 nm. The fluorescence spectra were obtained on a Horiba FluoroMax 4 spectrofluorometer. Raman spectra were recorded using a Raman microscope (Kaiser Optical Systems, Inc., Ann Arbor, MI, USA) with 785 nm laser excitation. The spectra were obtained for one 2 min exposure of the CCD detector in the wave-number range. X-ray powder diffraction was recorded on a D8 ADVANCE XRD (Bruker, Germany) with Cu $K\alpha$ radiation ($\lambda = 1.54056 \text{ \AA}$) at 40 mA and 45 kV. The sample was packed into a glass holder and diffraction patterns were collected over a 2θ range of 5–50, at a scan rate of 3 $^\circ \text{min}^{-1}$.

2.2. Synthesis of ligands L_1 and L_2

Synthesis of ligand L_1 4-(4-bromobenzylideneamino)-4H-1,2,4-triazole. Ligands L_1 and L_2 were synthesized according to the summary of the existing synthetic method, previously reported.^{22–26} The synthetic routes of compound L_1 are illustrated in Scheme S1 (ESI[†]). 10 mmol 4-bromobenzaldehyde (1.85 g) and 10 mmol 4-amino-4H-1,2,4-triazole (0.84 g) were dissolved in 80 mL ethanol, and then the resulting solution was refluxed at 80 $^\circ\text{C}$ for about 3 h. Concentration by rotary evaporation gave L_1

as a white solid. The white solid was collected by filtration, washed with ethanol and air-dried at room temperature (yield 65%). Elemental analysis anal. calcd (%): C, 43.05; N, 22.32; H, 2.81. Found: C, 43.07; N, 22.30; H, 2.82. IR (KBr, cm^{-1}): 3438, 3120, 1614, 1539, 1501, 1486, 1282, 824, 759.

Synthesis of ligand L_2 4-(4-iodobenzylideneamino)-4H-1,2,4-triazole. The synthetic routes of compound L_2 are illustrated in Scheme S2 (ESI[†]), and the synthesis method is similar to that of compound L_1 . 10 mmol 4-iodobenzaldehyde (2.32 g) and 10 mmol 4-amino-4H-1,2,4-triazole (0.84 g) were dissolved in 80 mL ethanol, and then the resulting solution was refluxed at 80 $^\circ\text{C}$ for about 3 h. Concentration by rotary evaporation gave L_2 as a yellow solid. The yellow solid was collected by filtration, washed with ethanol and air-dried at room temperature (yield 65%). Elemental analysis anal. calcd (%): C, 36.26; N, 18.80; H, 2.37. Found: C, 36.27; N, 18.82; H, 2.35. IR (KBr, cm^{-1}): 3437, 3117, 1615, 1583, 1533, 1483, 1164, 854, 819.

Ligands L_1 and L_2 were dissolved in a small amount of methanol solvent. The resulting clear solutions evaporated at room temperature after four days and single crystals of colorless and blocky L_1 crystals and light yellow blocky L_2 crystals suitable for X-ray diffraction were obtained.

2.3. Synthesis of organic salts 1–4

Synthesis of salts **1 and **2**.** The preparation of the salt was performed in solution by crystallization and pure methanol was used as the solvent. Salt **1** was obtained by dissolving a 3 : 5 stoichiometric ratio of L_1 (75.33 mg, 0.3 mmol) and HCl (47.97 mg, 0.5 mmol) in methanol under stirring at room temperature for twenty minutes and the resulting homogeneous solution was kept undisturbed at ambient temperature for slow evaporation. Elemental analysis anal. calcd (%): C, 37.59; N, 19.49; H, 2.80. Found: C, 37.60; N, 19.47; H, 2.82. IR (KBr, cm^{-1}): 3345, 3081, 2751, 2677, 1612, 1587, and 1088. Salt **2** was obtained in a similar way to salt **1** but using HClO_4 instead of HCl. Elemental analysis anal. calcd (%): C, 35.84; N, 18.60; H, 2.49. Found: C, 35.81; N, 18.62; H, 2.47.

Synthesis of salts **3 and **4**.** Salt **3** was obtained by dissolving a 3 : 5 stoichiometric ratio of L_2 (89.42 mg, 0.3 mmol) and HCl (47.97 mg, 0.5 mmol) in methanol under stirring at room temperature for twenty minutes and the resulting homogeneous solution was kept undisturbed at ambient temperature for slow evaporation. Elemental analysis anal. calcd (%): C, 32.31; N, 16.75; H, 2.41. Found: C, 32.34; N, 16.73; H, 2.40. Salt **4** was

Table 1 Crystal data and structural refinement for compounds **L**₁ and **L**₂ and crystals **2** and **3**

Compounds	L ₁	L ₂	2	3
Formula	C ₉ H ₇ N ₄ Br	C ₉ H ₇ N ₄ I	C ₁₈ H ₁₅ N ₈ O ₄ ClBr ₂	C ₉ H ₈ N ₄ ClI
Formula weight	251.10	298.09	602.65	334.54
Crystal system	Monoclinic	Monoclinic	Triclinic	Monoclinic
Space group	<i>P</i> 2 ₁ / <i>n</i>	<i>P</i> 2 ₁ / <i>n</i>	<i>P</i> $\bar{1}$	<i>P</i> 2 ₁ / <i>c</i>
<i>a</i> /Å	4.2810(9)	4.4720(9)	8.000(16)	9.5620(19)
<i>b</i> /Å	11.572(2)	11.701(2)	9.886(2)	6.6530(13)
<i>c</i> /Å	19.146(4)	19.032(4)	14.320(3)	17.748(4)
α /°	90.00	90.00	95.05(3)	90.00
β /°	93.49(3)	95.38(3)	97.80(3)	93.05(3)
γ /°	90.00	90.00	105.59(3)	90.00
<i>V</i> , Å ³	946.7(3)	991.5(3)	1071.5(4)	1127.5(4)
<i>Z</i>	4	4	2	4
<i>D</i> calc (Mg m ⁻³)	1.762	1.997	1.331	1.971
<i>T</i> /K	293(2)	293(2)	293(2)	293(2)
μ (mm ⁻¹)	4.304	3.194	3.953	3.049
Cryst dimensions	0.2 × 0.1 × 0.1	0.25 × 0.3 × 0.1	0.2 × 0.2 × 0.1	0.2 × 0.1 × 0.1
No. of refls collected	1733	1811	3893	2062
No. of unique refls	953	1191	2061	1618
No. of params	127	127	298	136
Goodness-of-fit on <i>F</i> ²	1.006	1.002	1.087	1.008
<i>R</i> ₁ , <i>wR</i> ₂ (<i>I</i> > 2 σ (<i>I</i>))	0.0546, 0.0903	0.0435, 0.0934	0.0896, 0.2170	0.0429, 0.1028
<i>R</i> ₁ , <i>wR</i> ₂ (all data)	0.1221, 0.1055	0.0797, 0.1052	0.1625, 0.2495	0.0588, 0.1101
CCDC No.	1519856	1519857	1519859	1519858

obtained using HClO₄ instead of HCl. Elemental analysis anal. calcd (%): C, 31.03; N, 16.09; H, 2.17. Found: C, 31.05; N, 16.07; H, 2.18.

2.4. X-ray crystallographic studies

The single-crystal X-ray diffraction data of compounds **L**₁ and **L**₂ and crystals **2** and **3** were collected at 293 K with graphite-monochromated Mo-K α radiation ($\lambda = 0.071073$ nm) equipped with a Rigaku SCXmini diffractometer.^{27,28} The lattice parameters were integrated using vector analysis and refined from the diffraction matrix; the absorption correction was carried out by using the Bruker SADABS program using the multi-scan method. The crystallographic data, data collection, and refinement parameters for compounds **L**₁ and **L**₂ are given in Table 1. The structures were solved using full-matrix least-squares methods on all *F*² data, and the SHELXS-2014 and SHELXL-2014 programs were used for structure solution and refinement, respectively.^{29,30} All non-hydrogen atoms were refined anisotropically and hydrogen atoms were geometrically fixed. The molecular graphics were prepared by using Mercury.³¹

3. Results and discussion

3.1. Crystal structures of ligands **L**₁ and **L**₂ and salts **2** and **3**

Shown in Fig. 1 are the crystal connecting motifs of ligands **L**₁ and **L**₂, and salts **2** and **3**. **L**₁ and **L**₂ were crystallized in the monoclinic *P*2₁/*n* space group, but the halogen-bonding interactions were different. The adjacent **L**₁ molecules are connected into a polymeric 1-D chain structure *via* the C–Br \cdots N halogen bonding interactions with the distances of Br \cdots N being 3.296 Å (Scheme 2). The chains are parallel to each other in a zigzag structure and different zigzag structures are linked in a parallel fashion to form a similar planar structure by $\pi\cdots\pi$ intermolecular interactions with a line separation of 2.889 Å. For crystal **L**₂, the

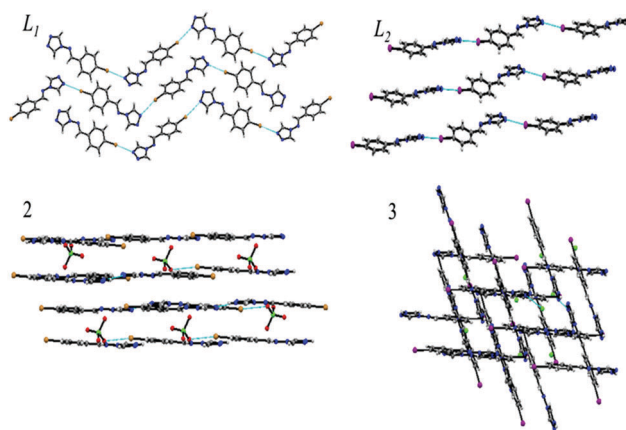
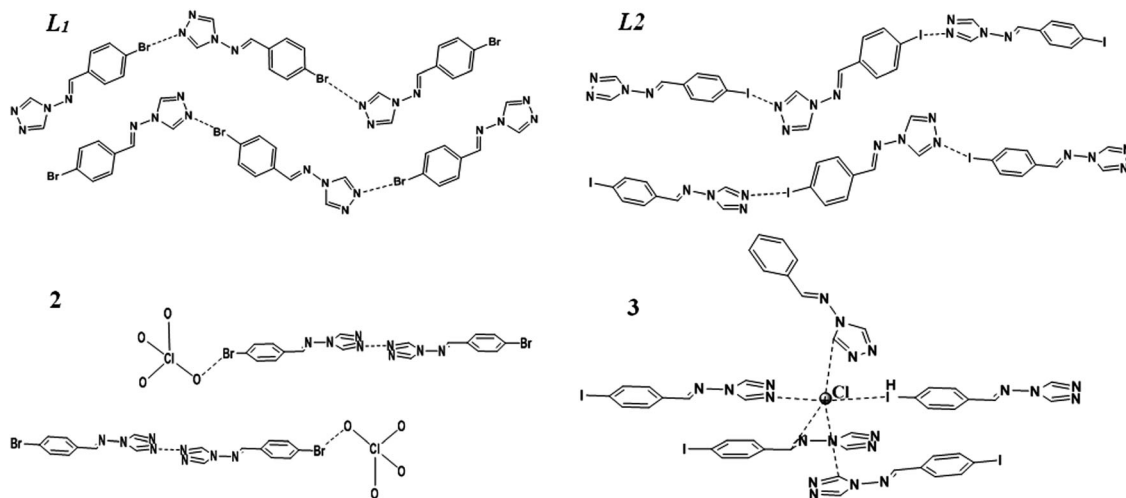


Fig. 1 The crystal packing of ligands **L**₁ and **L**₂ and crystals **2** and **3**.

halogen bonding connections are similar to those in **L**₁, but the halogen bonding C–I \cdots N is measured with distances of 3.210 Å (I \cdots N), which implies that the halogen-bonding interactions of I are stronger than those of Br, resulting in the molecules of **L**₂ adopting different stacking modes through weak $\pi\cdots\pi$ intermolecular interactions forming a stacked 3-D layered structure.

Crystal structural determinations reveal that **2** crystallizes in the triclinic *P* $\bar{1}$ space group; the asymmetric unit of **2** is composed of one protonated **L**₁, one **L**₁ molecule and one ClO₄[−] anion. **L**₁ molecules connect with ClO₄[−] anions into a 3-D frame structure through hydrogen-bonding and halogen-bonding interactions. In addition, because ClO₄[−] anions are an oxo-acid, hydrogen bonds play a major role in comparison to halogen bonds. The salt **2** molecules are connected by N₄–H \cdots N₈ interaction to form a tail–tail type interaction with one **L**₁ molecule connecting to a ClO₄[−] anion *via* C–Br₁ \cdots O₄ halogen-bonding interaction (Scheme 2). Salt **3** crystallizes in the monoclinic *P*2₁/*c* space group and the asymmetric unit is composed of one protonated



Scheme 2 The intermolecular hydrogen bonding and halogen bonding interactions have been marked.

L_2 molecule and one Cl^- anion (Scheme 1). For salt **3**, XB plays a significant role in crystal formation and the crystal structure. The Cl^- ion is five-connected being bonded to three carbon atoms [C_1 , C_2 and C_3] and one nitrogen atom [N_1] and one iodine atom [I]. The Cl^- ion, which plays a bridging role, connects the two protonated L_2 cations into a 1-D tail-face chain structure by infinite $\text{I} \cdots \text{Cl}$ halogen-bonding interaction (distance of 3.344 Å) and $\text{N}_1\text{-H} \cdots \text{Cl}$ hydrogen-bonding interaction (distance of 3.035 Å). At the same time, the Cl^- ion through weak $\text{C-H} \cdots \text{Cl}$ hydrogen bonding results in 2-D planes which are further interleaved into a 3-D network structure ($\text{C}_1\text{-H} \cdots \text{Cl} = 3.376$ Å and $\text{C}_2\text{-H} \cdots \text{Cl} = 3.544$ Å and $\text{C}_3\text{-H} \cdots \text{Cl} = 3.574$ Å). The geometrical parameters for the halogen bonds in ligands L_1 and L_2 and salts **2** and **3** are shown in Table S1 (ESI[†]). Both aromatic $\pi \cdots \pi$ stacking and halogen-bonding or hydrogen-bonding interactions together stabilize the structure.

For salts **1** and **4**, only crystalline powders were obtained, PXRD measurements (Fig. 2) revealed that the crystal structures of **1** and **4** are isostructural to **2** and **3**, due to the very similar

experimental X-ray powder diffraction patterns compared to those simulated from single crystals of **2** and **3**.

3.2. Thermal study

The thermal behaviors of ligands L_1 and L_2 and salts **1–4** were investigated on a Proteus Thermal analysis system (from NETZSCH TG 2009 F3) and the heating rate was around 20 K min^{-1} with the temperature range of 50–500 °C. Fig. 3 shows their TGA traces. The decomposition temperatures of ligands L_1 and L_2 are 250 °C and 262 °C, respectively, implying that the intermolecular halogen bonds of L_2 are stronger than those of L_1 . Salt **1** shows two steps of mass loss, the first mass loss step is in the temperature range of 138–200 °C (mass loss 15.47%), and the second decomposition is at a temperature of 254 °C with a loss of 58.23%, indicating the decomposition of ligand L_1 , which is similar to crystal **2**. Salt **3** shows a mass loss of 14.64% in the temperature range of 149–200 °C and further weight loss corresponds to the decomposition of L_2 at 262 °C. For salt **2**, due to serious hygroscopicity, the first weight loss is

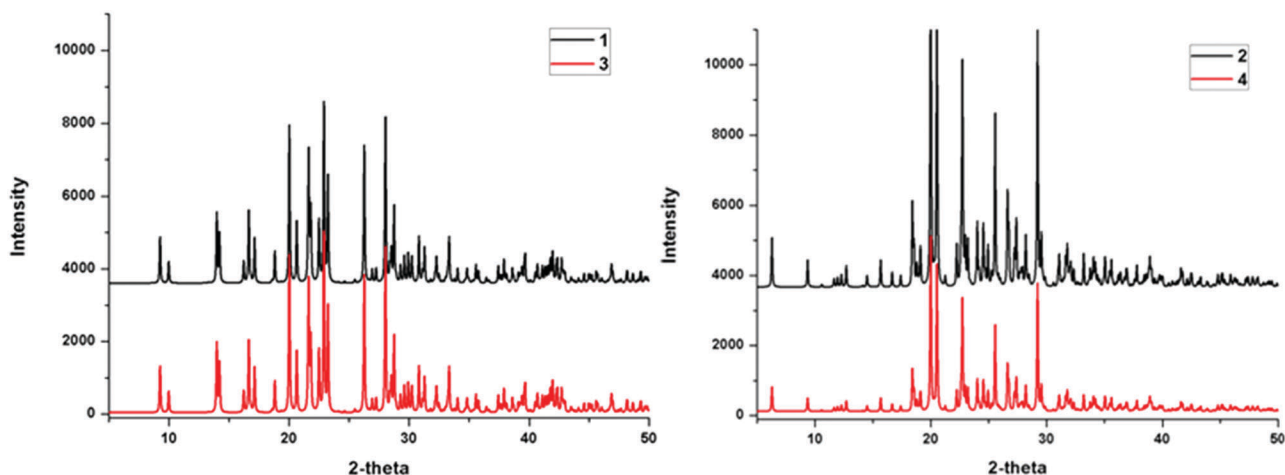


Fig. 2 PXRD patterns of salts **1–4**.

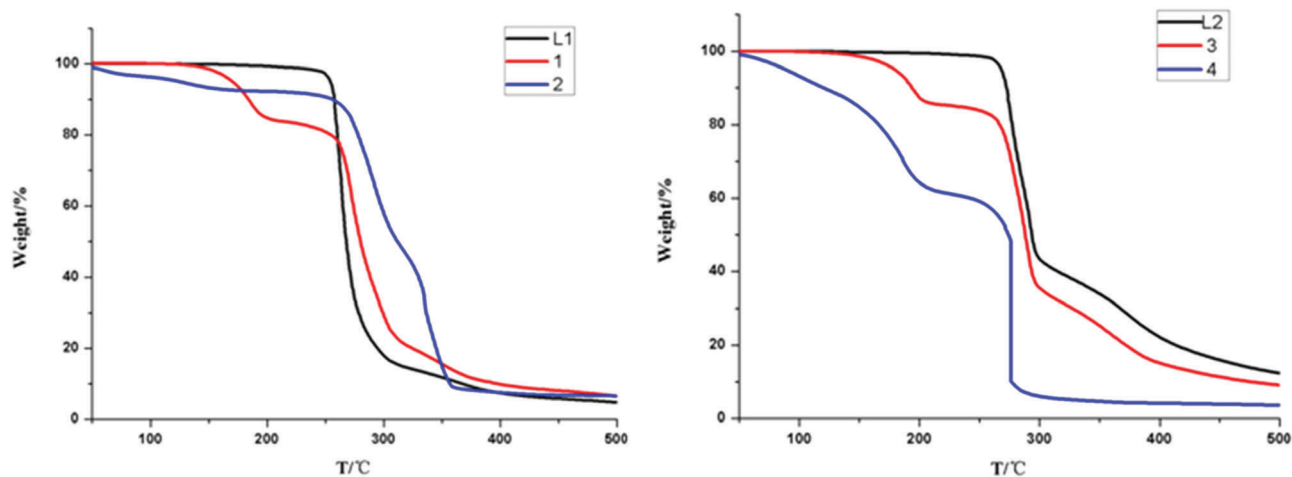


Fig. 3 TGA profiles of ligands L_1 and L_2 and salts **1–4** in the temperature range of 50–500 °C.

accompanied by the loss of free water molecules (mass loss 4.14%) and the next steps of weight loss above 264 °C are due to the disintegration and decomposition of the ligand L_1 molecules. For **4**, there is an obvious large weight loss above 50–200 °C (mass loss 42.13%). The second step of weight loss above 263 °C may be due to the decomposition of L_2 molecules, perchlorate anions and the collapse of the lattice structure. It can be seen that the characteristic decomposition temperatures of ligands L_1 and L_2 are reserved in halogen-bonding connected salts **1** and **3**, while they increase in hydrogen-bonding connected salts **2** and **4**.

3.3. Hirshfeld surface calculations

The Hirshfeld surface serves as a powerful tool for describing the surface characteristics of the molecules and identifying intermolecular interactions.³² The 3-D Hirshfeld d_{norm} surfaces and 2-D fingerprint plots of ligands L_1 and L_2 and salts **2** and **3** are shown in Fig. 4. The 3-D d_{norm} values are mapped onto the

Hirshfeld surface by using a red–blue–white color scheme: red regions represent closer contacts; blue regions represent longer contacts; and white regions represent the distance of contacts equal to vdW separation.^{33,34} The 3-D d_{norm} surfaces can be resolved into 2-D fingerprint plots, and the 2-D fingerprint plots are displayed by using the standard 0.4–2.6 Å view with the d_e and d_i distance scales displayed on the graph axes.

For L_1 and L_2 , the red regions on the d_{norm} surface are mainly concentrated around Br^- and I^- , corresponding to the $\text{Br} \cdots \text{N}$ and $\text{I} \cdots \text{N}$ halogen bonding interactions, and the $\text{N} \cdots \text{H}$ and $\text{C} \cdots \text{C}$ hydrogen bonding interactions also show a weak red region in L_1 and L_2 . For salt **2**, the red regions mainly represent the significant $\text{N} \cdots \text{H}$, $\text{O} \cdots \text{H}$ and $\text{Br} \cdots \text{O}$ interactions and these interactions comprise 14.2%, 22.6% and 4.7% to the total Hirshfeld surface, respectively. For **3**, $\text{I} \cdots \text{Cl}$ and $\text{Cl} \cdots \text{H}$ account for a large proportion of the red region in the total Hirshfeld surface, comprising 2.6% and 20.3%, respectively (all kinds of

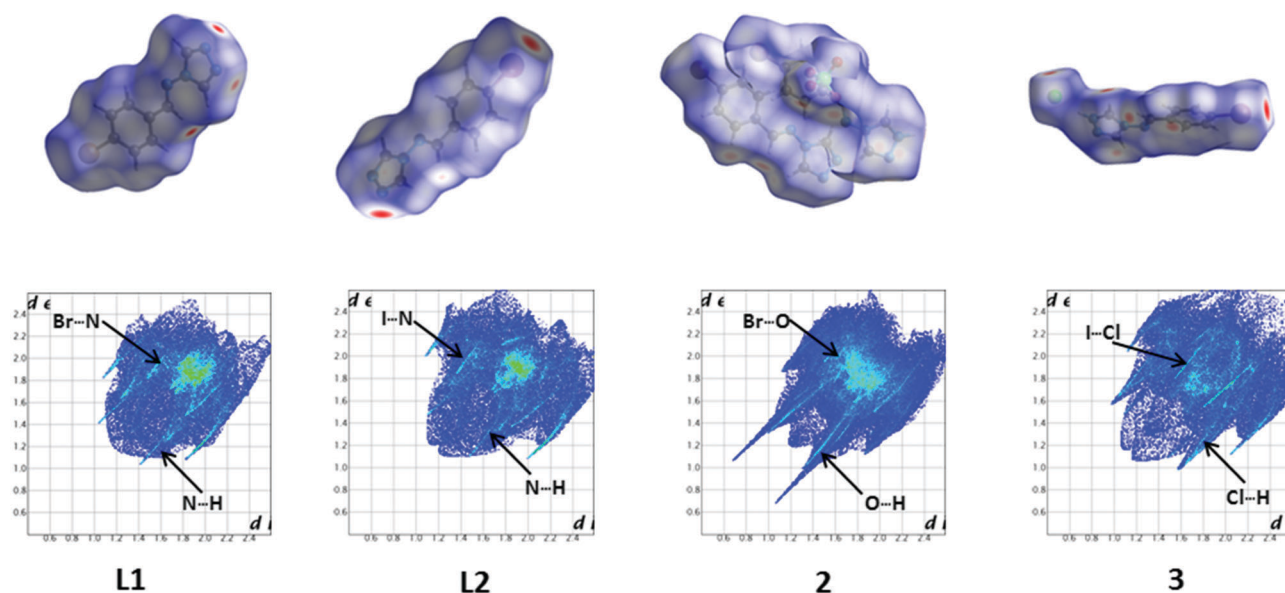


Fig. 4 Hirshfeld d_{norm} surfaces and 2-D fingerprint plots of ligands L_1 and L_2 , and salts **2** and **3**.

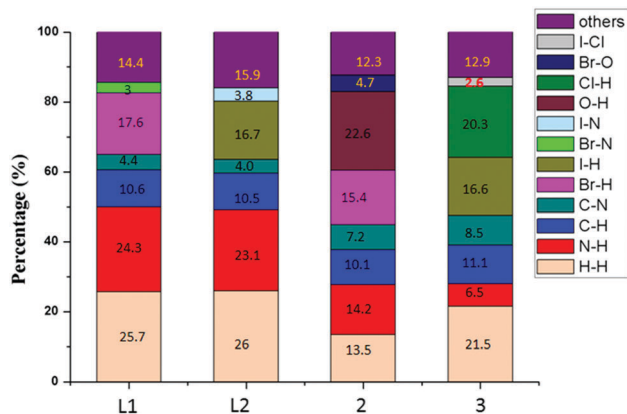


Fig. 5 The percentage contributions from the individual intermolecular interactions to the Hirshfeld surface of ligands L_1 and L_2 and salts **2** and **3**.

interactions are quantitatively summarized in Fig. 5). The above analysis shows that the halogen bond, similar to the hydrogen bond, plays an important role in the formation of crystal **3**, and halogen bonds account for more than hydrogen bonds. These results are in agreement with the X-ray crystallographic analysis of hydrogen-bonding and halogen-bonding interactions.

3.4. Raman spectroscopy

To investigate the peak change of compounds L_1 and L_2 after salt formation, we compared the Raman and IR spectra of compounds L_1 and L_2 and salts **1–4**. Fig. 6a shows Raman spectra in the region of $3300\text{--}40\text{ cm}^{-1}$. For L_1 , its characteristic peaks are around 3125 , 1507 , 881 , and 373 cm^{-1} . However, salts **1** and **2** have almost no influence on the characteristic peaks of L_1 apart from the disappearance of the peak at 1507 cm^{-1} due to the formation of halogen bonds and hydrogen bonds. Furthermore, salt **2** with a 3-D framework, has a distinct difference, as has been highlighted by rectangles in Fig. 6. The peak at around 453 cm^{-1} for **2** may be attributed to $\text{Br}\cdots\text{O}$

halogen bonds, and does not appear in ligand L_1 . For L_2 , a visible difference has been displayed in Fig. 6b between 3200 and 2995 cm^{-1} . This may be due to the inorganic anion by halogen-bonding with I affecting the fluorescence intensity of L_2 . The similar Raman profiles of ligands L_1 and L_2 and halogen-bonding connected salts **1** and **3** indicate that salt formation by halogen-bonding interaction has little effect on the vibrations of ligand functional groups, which also was confirmed by the IR spectra (Fig. S1, ESI[†]).

3.5. Fluorescence spectra

To further investigate the effect of halogen-bonding contacts on organic salts, fluorescence emission spectra studies were carried out. The emission spectra of the six compounds in methanol are shown in Fig. 7 and the excitation wavelength is 285 nm . By comparing the fluorescence emission spectra of the four salts and the corresponding ligand in solution, which is ligand L_1 , salts **1** and **2** exhibit emissions with maximum peaks (λ_{max}) at around 372 nm in solution, and for ligand L_2 , salts **3** and **4** at 370 nm have a maximum emission peak; it can be seen that the fluorescence emissions of salts **1** and **3** are probably assigned to the intra-ligand fluorescence emission because similar behaviors are also observed for the free ligands L_1 and L_2 , respectively, and halogen bonding contacts account for the major part among the salts and ligands in methanol solution. Besides, this can be further confirmed using UV-visible absorption spectra in solution as reported in this paper (Fig. S2, ESI[†]).

Compared with the similar maximum fluorescence peaks (λ_{max}) in methanol solution, the fluorescence spectra of all the salts in the solid state displayed strong and red-shifted emissions using the excitation wavelength at 373 nm (Fig. 8). Intermolecular vibrational relaxation is effectively inhibited, which would cause strong shifted emissions in the solid state compared with those in solution.³⁵ Furthermore, after introducing the conjugated aromatic aldehyde structure into 4-amino-1,2,4-triazole, the fluorescence efficiency increases with increasing conjugation

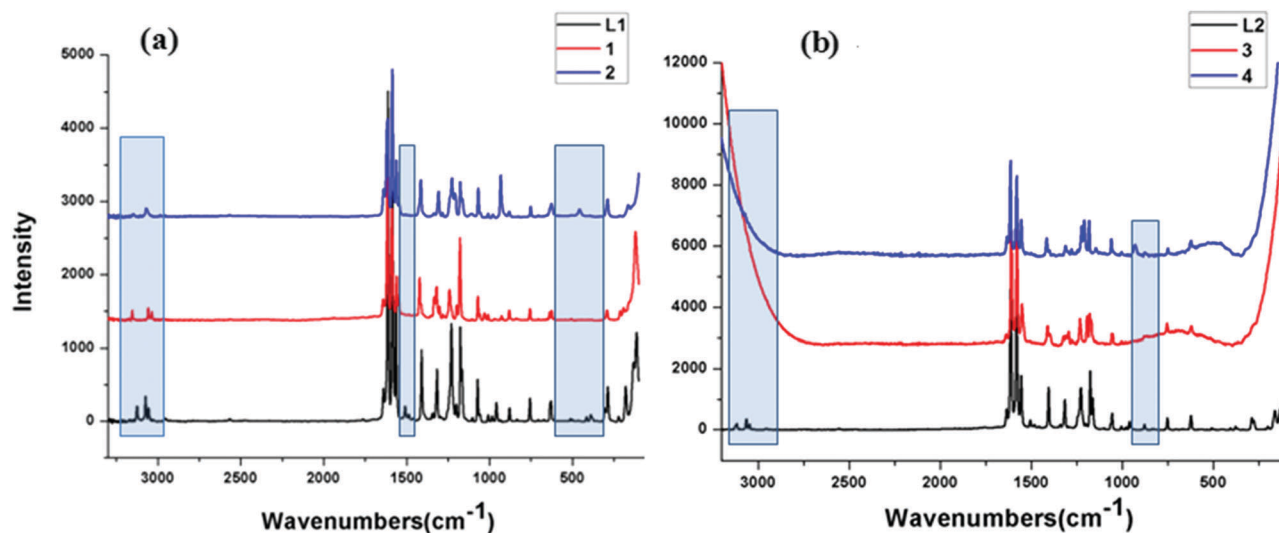


Fig. 6 Raman spectra of complexes L_1 and L_2 and salts **1–4**. The differences are highlighted.

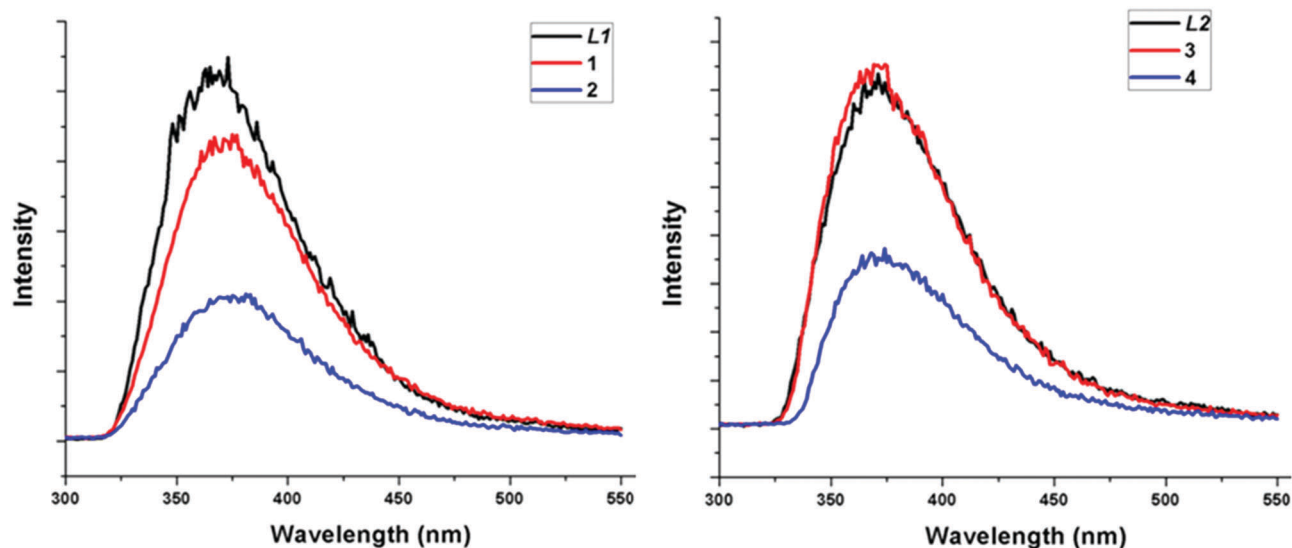


Fig. 7 Fluorescence emission spectra of ligands L_1 and L_2 and salts **1–4** in methanol solution ($2.5 \times 10^{-5} \text{ mol L}^{-1}$).

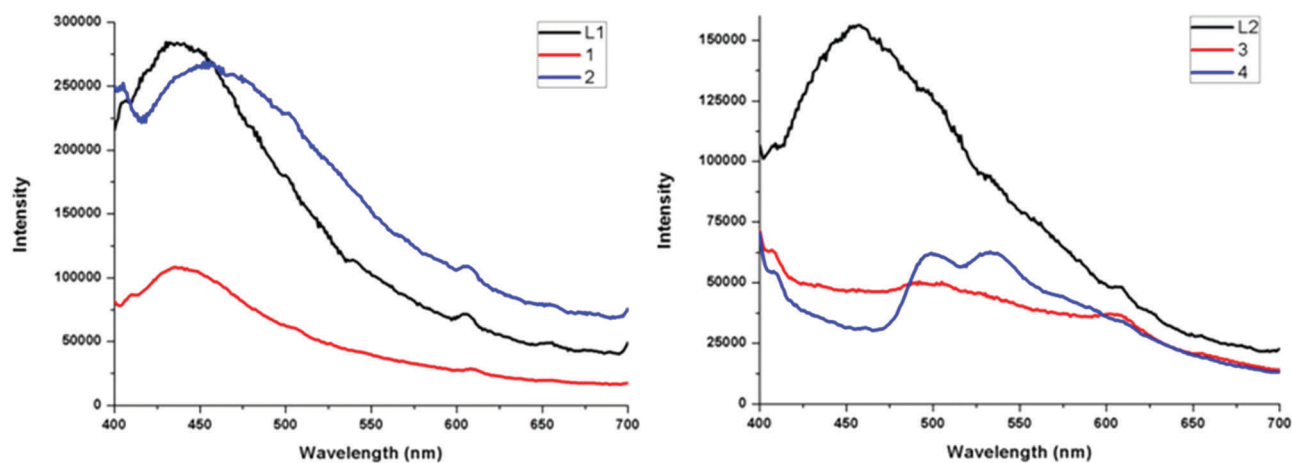


Fig. 8 Fluorescence emission spectra of ligands L_1 and L_2 and salts **1–4** in the solid state.

of π electrons and molecular flatness, and the fluorescence spectrum moves in the long wavelength direction. Salts **1** and **2** have a maximum emission peak at 435 nm and 456 nm, respectively, which shows a slight red-shift compared to that of ligand L_1 at 432 nm. Salts **3** and **4** show a visible change compared to ligand L_2 and salt **4** even has two fluorescence emission peaks, which implies that different anions have different influences on the fluorescence properties of the ligand in the solid state. The connection and strength are also different; from the above analysis, it can be seen that the halogen bond plays a major role in salts **1** and **3**, in the same way as the ligand, while the hydrogen bond occupies a larger proportion in **2** and **4**. In addition, the red-shifted and reduced intensity of the fluorescence of the salts can be ascribed to the increase of conjugation of π electrons, where the ligands with anions are linked mainly by halogen bonds in **1** and **3** and through hydrogen bonds in **2** and **4**. Comparing the fluorescence spectra of the ligand and the corresponding salts in solution and in the solid state indicates that the

fluorescence properties of ligands L_1 and L_2 are reserved in halogen-bonding connected salts **1** and **3**, while change and reduction in hydrogen-bonding connected salts **2** and **4**.

4. Conclusions

In summary, $\text{HL}_1^+\cdot\text{Cl}^-$ (**1**), $\text{L}_1\cdot\text{HL}_1^+\cdot\text{ClO}_4^-$ (**2**), $\text{HL}_2^+\cdot\text{Cl}^-$ (**3**), and $\text{L}_2\cdot\text{HL}_2^+\cdot\text{ClO}_4^-$ (**4**), based on the new ligands 4-(4-bromobenzylideneamino)-4*H*-1,2,4-triazole (L_1) and 4-(4-iodobenzylideneamino)-4*H*-1,2,4-triazole (L_2), have been successfully synthesized and the influence of halogen-bonding contacts on the crystal structure and the fluorescence properties of these organic salts has been investigated. Compounds L_1 and L_2 exhibit a polymeric 1-D chain in zigzag structures *via* C–Br \cdots N and C–I \cdots N halogen-bonding interactions. For salt **2**, N–H \cdots O hydrogen-bonding contacts play a major role, resulting in a 3-D framework structure. Each Cl^- ion connects to three carbon atoms,

one nitrogen atom and the one iodine atom; meanwhile, the Cl⁻ ion using C-I...Cl halogen-bonding results in an interleaved 3-D network structure of **3**. The results of the luminescence properties reveal that compared with hydrogen-bonding contacts, halogen-bonding contacts can lead to preservation of the emission intensity of the ligand in salts **1** and **3**, while reducing the emission intensity in hydrogen-bonding connected salts **2** and **4**. This work may provide a better understanding of the role of halogen-bonding contacts in tuning the photo-physical properties of organic salts.

Acknowledgements

This research was based on work supported by the Fundamental Research Funds for the Central Universities (No. 3207047407), Natural Science Foundation of China (Grant No. 21371031 and 21628101), International S&T Cooperation Program of China (No. 2015DFG42240) and the Priority Academic Program Development (PAPD) of Jiangsu Higher Education Institutions.

References

- (a) H. S. Azevedo and I. Pashkuleva, *Adv. Drug Delivery Rev.*, 2015, **94**, 63; (b) Y.-H. Luo, D.-E. Wu, G.-J. Wen, L.-S. Gu, L. Chen, J.-W. Wang and B.-W. Sun, *ChemistrySelect*, 2017, **2**(1), 614.
- (a) J.-W. Wang, Y.-W. Zhang, M.-X. Wang, Y.-H. Luo and B.-W. Sun, *Polyhedron*, 2017, **124**, 243; (b) Y.-H. Luo, Y. Sun, Q.-I. Liu, L.-J. Yang, G.-J. Wen, M.-X. Wang and B.-W. Sun, *ChemistrySelect*, 2016, **1**(13), 3879.
- (a) A. Alshammari, M. G. Posner, A. Upadhyay, F. Marken, S. Bagby and A. Ilie, *ACS Appl. Mater. Interfaces*, 2016, **8**(32), 21077; (b) D. Quinonero, I. Alkorta and J. Elguero, *Phys. Chem. Chem. Phys.*, 2016, **18**(40), 27939; (c) G. Kawaguchi, M. Maesato, T. Komatsu, T. Imakubo, A. Kiswandhi, D. Graf and H. Kitagawa, *Chem. Mater.*, 2016, **28**(20), 7276.
- (a) Y.-H. Luo, J.-W. Wang, C. Chen, Y.-J. Li and B.-W. Sun, *Cryst. Growth Des.*, 2017, **17**, 2576; (b) R. S. Mulliken and W. B. Person, *Molecular Complexes: A Lecture and Reprint Volume*, Wiley-Interscience, New York, 1969.
- R. S. Mulliken, *Spectroscopy, Molecular Orbitals, and Chemical Bonding*.
- O. Hassel, *Structural Aspects of Interatomic Charge-Transfer Bonding*.
- (a) Y.-H. Luo, J.-W. Wang, Y.-J. Li, C. Chen, P.-J. An, S.-L. Wang, C.-Q. You and B.-W. Sun, *CrystEngComm*, 2017, **19**(24), 3362–3369; (b) F. Guthrie, *J. Chem. Soc.*, 1863, **16**, 239–244.
- A. Priimagi, G. Cavallo, P. Metrangolo and G. Resnati, *Acc. Chem. Res.*, 2013, **46**, 2686–2695.
- G. Cavallo, P. Metrangolo, R. Milani, T. Pilati, A. Priimagi, G. Resnati and G. Terraneo, *Chem. Rev.*, 2016, **116**, 2478–2601.
- (a) N. K. Beyeh, M. Cetina and K. Rissanen, *Chem. Commun.*, 2014, **50**, 1959; (b) L. Turunen, N. K. Beyeh, F. Pan, A. Valkonen and K. Rissanen, *Chem. Commun.*, 2014, **50**, 15920; (c) P. Metrangolo, J. S. Murray, T. Pilati, P. Politzer, G. Resnati and G. Terraneo, *CrystEngComm*, 2011, **13**, 6593; (d) R. Liantonio, P. Metrangolo, T. Pilati, G. Resnati and A. Stevenazzi, *Cryst. Growth Des.*, 2003, **3**, 799; (e) L. Russo, S. Biella, M. Lahtinen, R. Liantonio, P. Metrangolo, G. Resnati and K. Rissanen, *CrystEngComm*, 2007, **9**, 341.
- (a) P. Metrangolo and G. Resnati, *Chem. – Eur. J.*, 2001, **7**, 2511; (b) D. E. Barry, C. S. Hawes, S. Blasco and T. Gunnlaugsson, *Cryst. Growth Des.*, 2016, 5194.
- A. Crihfield, J. Hartwell, D. Phelps, R. B. Walsh, J. L. Harris, J. F. Payne, W. T. Pennington and T. W. Hanks, *Cryst. Growth Des.*, 2003, **3**, 313.
- O. S. Bushuyev, T. Friscic and C. J. Barrett, *Cryst. Growth Des.*, 2016, **16**, 541–545.
- (a) M. Carter, A. R. Voth, M. R. Scholfield, B. Rummel, L. C. Sowers and P. S. Ho, *Biochemistry*, 2013, **52**, 4891; (b) A. R. Voth, P. Khuu, K. Oishi and P. S. Ho, *Nat. Chem.*, 2009, **1**, 74.
- (a) T. Kusamoto, H. M. Yamamoto and R. Kato, *Cryst. Growth Des.*, 2013, **13**, 4533; (b) T. Imakubo, T. Shirahata, K. Hervé and L. Ouahab, *J. Mater. Chem.*, 2005, **16**, 162.
- (a) E. Cariati, A. Forni, S. Biella, P. Metrangolo, F. Meyer, G. Resnati, S. Righetto, E. Tordina and R. Ugo, *Chem. Commun.*, 2007, 2590; (b) B. K. Saha, A. Nangia and J. F. Nicoud, *Cryst. Growth Des.*, 2006, **6**, 1278.
- F. Kniep, S. H. Jungbauer, Q. Zhang, S. M. Walter, S. Schindler, I. Schnapperelle, E. Herdtweck and S. M. Huber, *Angew. Chem., Int. Ed.*, 2013, **52**, 7028.
- (a) L. C. Gilday, N. G. White and P. D. Beer, *Dalton Trans.*, 2013, **42**, 15766; (b) B. R. Mullaney, A. L. Thompson and P. D. Beer, *Angew. Chem., Int. Ed.*, 2014, **53**, 11458; (c) P. Metrangolo, T. Pilati, G. Terraneo, S. Biella and G. Resnati, *CrystEngComm*, 2009, **11**, 1187.
- H. L. Nguyen, P. N. Horton, M. B. Hursthouse, A. C. Legon and D. W. Bruce, *J. Am. Chem. Soc.*, 2004, **126**, 16.
- S. Saha and G. R. Desiraju, *J. Am. Chem. Soc.*, 2017, **139**, 1975–1983.
- C. Bosshard, M. S. Wong, F. Pan, P. Ggnter and V. Gramlich, *Adv. Mater.*, 1997, **9**, 554.
- (a) B. Belghoul, I. Welterlich, A. Maier, A. Toutianoush, A. R. Rabindranath and B. Tieke, *Langmuir*, 2007, **23**, 5062; (b) P. L. Zhao, P. Chen, Q. Li, M. J. Hu, P. C. Diao, E. S. Pan and W. W. You, *Bioorg. Med. Chem. Lett.*, 2016, **26**, 3679.
- P. S. Hariharan and S. P. Anthony, *Anal. Chim. Acta*, 2014, **848**, 74.
- H. Yuan, Q. Q. Li, H. Li, Q. N. Guo, Y. G. Lu and Z. Y. Li, *Dalton Trans.*, 2010, **39**, 11344.
- H. D. Bian, W. Gu, J. Y. Xu, F. Bian, S. P. Yan, D. Z. Liao, Z. H. Jiang and P. Cheng, *Inorg. Chem.*, 2003, **42**, 4265.
- C. Núñez, C. Silva López, O. N. Faza, F. L. Javier, M. Diniz, R. Bastida, J. L. Capelo and C. Lodeiro, *J. Biol. Inorg. Chem.*, 2013, **18**, 679.
- (a) Y. H. Luo, L. J. Yang, Q. L. Liu, Y. Ling, Y. Sun, J. W. Wang, C. Q. You and B. W. Sun, *J. Mater. Chem. C*, 2016, **4**, 8061; (b) Y. H. Luo, M. Nihei, G. J. Wen, B. W. Sun and H. Oshio, *Inorg. Chem.*, 2016, **55**, 8147.
- Yarnton, Oxfordshire. Agilent Technologies (formerly Oxford Diffraction). England, 2012.
- G. M. Sheldrick, *Acta Crystallogr.*, 2015, **3**, C71.

- 30 Rigaku, *CrystalClear, Version 14.0*, Rigaku Corporation, Tokyo, Japan, 2005.
- 31 Mercury 2.3 Supplied with Cambridge Structural Database, CCDC, Cambridge, UK, 2003–2004.
- 32 (a) F. P. A. Fabbiani, L. T. Byrne, J. J. McKinnon and M. A. Spackman, *CrystEngComm*, 2007, **9**, 728; (b) M. A. Spackman and J. J. McKinnon, *CrystEngComm*, 2002, **4**, 378.
- 33 Y.-H. Luo, G.-J. Wen, L.-S. Gu, M.-N. Wang and B.-W. Sun, *Polyhedron*, 2017, **121**, 101.
- 34 Y.-H. Luo, C. Chen, Y.-J. Li, J.-W. Wang and B.-W. Sun, *Dyes Pigm.*, 2017, **143**, 239.
- 35 (a) S. Kim, Q. D. Zheng, G. S. He, D. J. Bharali, H. E. Pudavar, A. Baev and P. N. Prasad, *Adv. Funct. Mater.*, 2006, **16**, 2317; (b) W. Retting, *Angew. Chem., Int. Ed.*, 1986, **25**, 971.